mTOR-Dependent Synapse Formation Underlies the Rapid Antidepressant Effects of NMDA Antagonists

B1) that colocalized with linear arrays of GFP-mini-N2G (Fig. 3C and fig. S14). Expressed GFP-SUN2 also formed linear arrays on the dorsal surface of nuclei (fig. S15). Because the linear arrays are actin-dependent, specific molecular assemblies of nesprin2G and SUN2 and not deformations of the nuclear envelope, we refer to them as TAN (transmembrane actin-associated nuclear) lines.

SUN2 depletion also inhibited nuclear positioning and centrosome orientation (Fig. 3D and figs. S4 and S16). Unlike other nuclear envelope proteins examined, nesprin2G levels and nuclear localization were reduced by SUN2 depletion (fig. S4). Expressed GFP-SUN2, but not GFP-SUN1, rescued the polarity defects in SUN2-depleted cells. These results indicate that SUN1 and SUN2 are not functionally equivalent for nuclear movement (Fig. 3D and fig. S16). GFP-mini-N2G expression in SUN2-depleted cells failed to restore centrosome orientation and nuclear positioning, further suggesting that nesprin2G requires SUN2 for normal nuclear movement (Fig. 3D and fig. S16).

During nuclear movement, GFP-mini-N2G TAN lines were observed moving rearward with the nucleus and dorsal actin cables labeled with Lifeact-mCherry (Fig. 4, A to D, fig. S17, and movies S6 and S7). Velocity measurements confirmed this correlation for many moving nuclei (Fig. 4C). Dual imaging of GFP-TAN lines and Lifeact-mCherry additionally revealed that TAN lines formed after dorsal cables (Fig. 4D, arrows). Thus, actin organizes TAN lines, which may form to functionally harness the force of retrograde actin flow for nuclear movement.

Centrosome orientation has been implicated in directed cell migration (5, 16). We determined whether inhibition of centrosome orientation by disrupting nuclear movement affected cell migration. Nesprin2G- or SUN2-depleted cells migrated into in vitro wounds slower than control cells did, consistent with previous results (fig. S18, A and B) (12). Furthermore, wound-edge cells expressing RFP-KASH fell behind the wound edge compared with cells expressing control constructs (fig. S19, C and D). Thus, the LINC complex and nuclear movement is required for efficient cell migration.

Here, the LINC complex components nesprin2G and SUN2 were found to assemble into TAN lines that provide a direct linkage between the nucleus and retrograde moving dorsal actin cables. Because each component of the TAN lines (nesprin2G, SUN2, and actin cables) was required for nuclear movement and TAN lines moved with dorsal cables during nuclear movement, we suggest that this assembly transmits force from retrograde actin flow to the nucleus. The accumulation of multiple nesprin2G and SUN2 molecules along an actin cable may be necessary to resist forces exerted by retrograde actin flow. Analogous force-resisting mechanisms were proposed for yeast KASH and SUN protein arrays, although these appear as spotwelds and anchor microtubules to the nuclear envelope (23).

We propose that TAN lines are functionally analogous to focal adhesions, which are clustered transmembrane integrins and associated cytoplasmic proteins that link the extracellular matrix to actin filaments. Both structures assemble in response to actin bundling by nonmuscle myosin II, and both transmit force across membranes. Unlike focal adhesions, TAN lines span two membranes and form along the length of an actin cable. Because INM SUN2 does not directly contact cytoplasmic dorsal actin cables, a regulatory "outside-in" signaling pathway, analogous to that for integrins (24), may exist that allows SUN2 to recognize nesprin2G engaged with actin and assembled into TAN lines. Recent work in mice suggests that nesprins and SUNs are important for normal mammalian development (13, 25, 26). It will be interesting to explore whether these proteins need to form a macromolecular structure like TAN lines to function during development.

References and Notes

1. S. Reinsch, P. Gönczy, *J. Cell Sci.* **111**, 2283 (1998).
2. D. A. Starr, *J. Cell Sci.* **122**, 577 (2009).
3. K. Wilhelmsen, M. Ketema, H. Truong, A. Sonnenberg, *J. Cell Sci.* **119**, 5021 (2006).
4. F. Del Bene, A. M. Wehman, B. A. Link, H. Baier, *Cell* **134**, 1055 (2008).
5. E. R. Gomes, S. Jani, G. G. Gundersen, *Cell* **121**, 451 (2005).
6. M. B. Goulding, J. C. Canman, E. N. Senning, A. H. Marcus, B. Bowerman, *J. Cell Biol.* **178**, 1177 (2007).
7. T. Ketelaar *et al.*, *Plant Cell* **14**, 2941 (2002).
8. S. L. Ramos-García, R. W. Roberson, M. Freitag, S. Bartnicki-García, R. R. Mouriño-Pérez, *Eukaryot. Cell* **8**, 1880 (2009).
9. D. J. Solecki *et al.*, *Neuron* **63**, 63 (2009).
10. J. W. Tsai, K. H. Bremner, R. B. Vallee, *Nat. Neurosci.* **10**, 970 (2007).
11. M. Crisp *et al.*, *J. Cell Biol.* **172**, 41 (2006).
12. Y. Lüke *et al.*, *J. Cell Sci.* **121**, 1887 (2008).
13. X. Zhang *et al.*, *Neuron* **64**, 173 (2009).
14. Materials and methods are available as supporting material on *Science* Online.
15. D. A. Starr, M. Han, *Science* **298**, 406 (2002).
16. J. Schmoranzer *et al.*, *Curr. Biol.* **19**, 1065 (2009).
17. A. J. Ridley, A. Hall, *Cell* **70**, 389 (1992).
18. A. J. Ridley, H. F. Paterson, C. L. Johnston, D. Diekmann, A. Hall, *Cell* **70**, 401 (1992).
19. P. Naumanen, P. Lappalainen, P. Hotulainen, *J. Microsc.* **231**, 446 (2008).
20. J. P. Heath, *Cell Biol. Int. Rep.* **5**, 975 (1981).
21. J. P. Heath, *J. Cell Sci.* **60**, 331 (1983).
22. J. Riedl *et al.*, *Nat. Methods* **5**, 605 (2008).
23. M. C. King, T. G. Drivas, G. Blobel, *Cell* **134**, 427 (2008).
24. K. R. Legate, S. A. Wickström, R. Fässler, *Genes Dev.* **23**, 397 (2009).
25. K. Lei *et al.*, *Proc. Natl. Acad. Sci. U.S.A.* **106**, 10207 (2009).
26. X. Zhang *et al.*, *Development* **134**, 901 (2007).
27. A. F. Palazzo *et al.*, *Curr. Biol.* **11**, 1536 (2001).
28. We thank W. Dauer, H. Herrmann, E. Marcantonio, G. Morris, S. Shackleton, R. Wedlich-Soldner, and H. Worman for providing reagents; members of the Dauer, Hirano, and Worman labs for helpful discussions; and Y. Zhao for analysis. This work was supported by a Dystonia Medical Research Foundation Fellowship (G.W.G.L.), an American Heart Association fellowship (E.S.F.), a Muscular Dystrophy Association grant (E.R.G.), an Association pour la Recherche sur le Cancer grant (E.R.G.), a Ligue Nacionale contre le Cancer grant (E.R.G.), a Dystonia Medical Research Foundation grant (G.G.G.), and NIH (GM06929 and NS059352) grants (G.G.G.).

---

mTOR-Dependent Synapse Formation Underlies the Rapid Antidepressant Effects of NMDA Antagonists

Nanxin Li, Boyoung Lee, Rong-Jian Liu, Mounira Banasr, Jason M. Dwyer, Masaaki Iwata, Xiao-Yuan Li, George Aghajanian, Ronald S. Duman*

The rapid antidepressant response after ketamine administration in treatment-resistant depressed patients suggests a possible new approach for treating mood disorders compared to the weeks or months required for standard medications. However, the mechanisms underlying this action of ketamine [a glutamate N-methyl-D-aspartic acid (NMDA) receptor antagonist] have not been identified. We observed that ketamine rapidly activated the mammalian target of rapamycin (mTOR) pathway, leading to increased synaptic signaling proteins and increased number and function of new spine synapses in the prefrontal cortex of rats. Moreover, blockade of mTOR signaling completely blocked ketamine induction of synaptogenesis and behavioral responses in models of depression. Our results demonstrate that these effects of ketamine are opposite to the synaptic deficits that result from exposure to stress and could contribute to the fast antidepressant actions of ketamine.

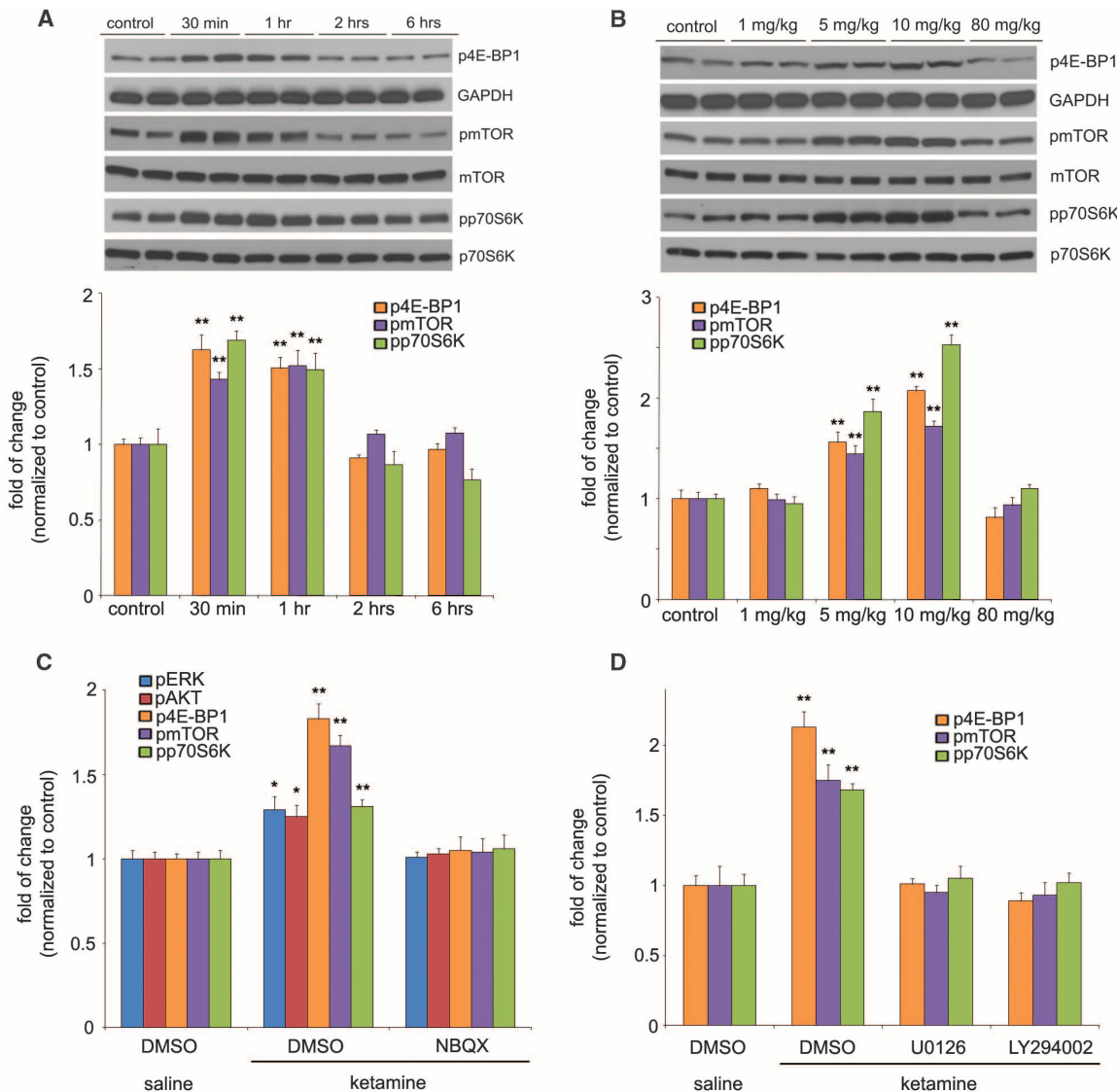Major depressive disorder (MDD) afflicts about 17% of the population and is one of the leading causes of total disability and economic burden (1). Although there are medications that alleviate depressive symptoms, these have serious limitations. Most notably, available

treatments require weeks or months to produce a therapeutic response, and only about one-third of patients respond to the first medication prescribed (2). In contrast, recent studies demonstrate that a single, low dose of a glutamate N-methyl-D-aspartic acid (NMDA) receptor antagonist produces a rapid (within hours) antidepressant response that lasts

Laboratory of Molecular Psychiatry, Center for Genes and Behavior, Departments of Psychiatry and Neurobiology, Yale University School of Medicine, 34 Park Street, New Haven, CT 06508, USA.

*To whom correspondence should be addressed. E-mail: ronald.duman@yale.edu

for up to 7 days (3, 4) and is effective in MDD patients who are resistant to traditional antidepressants (5). The mechanisms underlying rapid antidepressant actions are likely more complicated than simple NMDA receptor blockade and so far have not been identified. We carried out a series of studies to examine the cellular signaling pathways that mediate the behavioral actions of NMDA receptor blockade, focusing on signaling cascades known to rapidly influence synaptic plasticity (6).

The drug used for clinical trials is ketamine, a nonselective NMDA receptor antagonist (7). A low dose of ketamine (10 mg/kg), which is re-

ported to have antidepressant actions in behavioral models of depression (7), rapidly activated the mammalian target of rapamycin (mTOR) signaling pathway in the prefrontal cortex (PFC) of rats (Fig. 1A). Activation of mTOR signaling was observed in a preparation enriched in synaptoneurosomes (fig. S1) and included increased levels of the phosphorylated and activated forms of eukaryotic initiation factor 4E binding protein 1 (4E-BP1), p70S6 kinase (p70S6K), and mTOR (Fig. 1A). Increased phosphorylation of 4E-BP1, p70S6K, and mTOR is transient, returning to basal levels by 2 hours after ketamine administration (Fig. 1A). In contrast, other antidepressants

Fig. 1. Ketamine transiently and dose-dependently activates mTOR signaling in rat PFC. Values represent mean ± SEM [$n = 4$ animals; $*P < 0.05$; $**P < 0.01$; analysis of variance (ANOVA)]. (**A**) Time course of ketamine [10 mg/kg, intraperitoneally (ip)]–induced mTOR signaling determined by Western blot analysis of phospho-mTOR (pmTOR), phospho-4E-BP1 (p4E-BP1), and phospho-p70S6K (pp70S6K) in synaptoneurosomes of PFC. Levels of total mTOR, glyceraldehyde-3-phosphate dehydrogenase (GAPDH), and p70S6K were also determined. (**B**) Dose-dependent activation, determined 1 hour after ketamine administration, of pmTOR,

p4E-BP1, and pp70S6K. (**C**) Pretreatment (10 min) with NBQX (10 mg/kg, ip) blocked ketamine (10 mg/kg, ip) activation of pmTOR, p4E-BP1, and pp70S6K, as well as upstream signaling kinases phospho-ERK (pERK) and phospho-Akt (pAkt) (analyzed 1 hour after ketamine). Levels of pERK1 and pERK2 were similarly regulated and were combined for quantitative analysis. DMSO, dimethyl sulfoxide. (**D**) Pretreatment (30 min) with inhibitors of ERK (U0126, 20 nmol, ICV) or PI-3k/Akt (LY294002, 20 nmol, ICV) abolished ketamine (10 mg/kg, ip) activation of mTOR signaling proteins (analyzed 1 hour after ketamine administration).

tested, including electroconvulsive seizure, imipramine, or fluoxetine, did not significantly influence mTOR signaling (fig. S2). Ketamine produced a similar rapid and transient increase in the phosphorylated and activated forms of extracellular signal–regulated kinase (ERK, including ERK1 and ERK2) and protein kinase B (PKB/Akt) (fig.

S3A), growth factor signaling pathways that have been linked to activation of mTOR signaling (8). The activation of 4E-BP1, p70S6K, mTOR (Fig. 1B), ERK, and Akt (fig. S3B) was dose dependent, occurring at relatively low doses (5 to 10 mg/kg) that produce antidepressant behavioral actions but not at a higher anesthetic dose (7).

The antidepressant actions of ketamine have been reported to require glutamate α-amino-3-hydroxy-5-methyl-4-isoxazolepropionic acid receptor (AMPA) receptors (7). In line with this, we found that pretreatment (10 min) with a selective AMPA receptor inhibitor, 2,3-dihydroxy-6-nitro-7-sulfamoyl-benzo[f]quinoxaline-2,3-dione (NBQX),

Fig. 2. Ketamine rapidly increases synaptic proteins and spine number. (**A**) Time course for ketamine (10 mg/kg, ip) induction of synaptic proteins Arc, synapsin I, PSD95, and GluR1 in synaptoneurosomes of PFC and (**B**) blockade by pretreatment (30 min) with a selective mTOR inhibitor, rapamycin (0.2 nmol, ICV) (values represent mean ± SEM, n = 4 to 6 animals; *$P < 0.05$; **$P < 0.01$; ANOVA). (**C**) Ketamine-increased spine density in mPFC, analyzed by two-photon microscopy 24 hours after treatment. Representative images are shown of high-magnification Z-stack projections of apical tuft segments of neurobiotin-labeled layer V pyramidal cells (scale bar indicates 5 μm). (**D**)
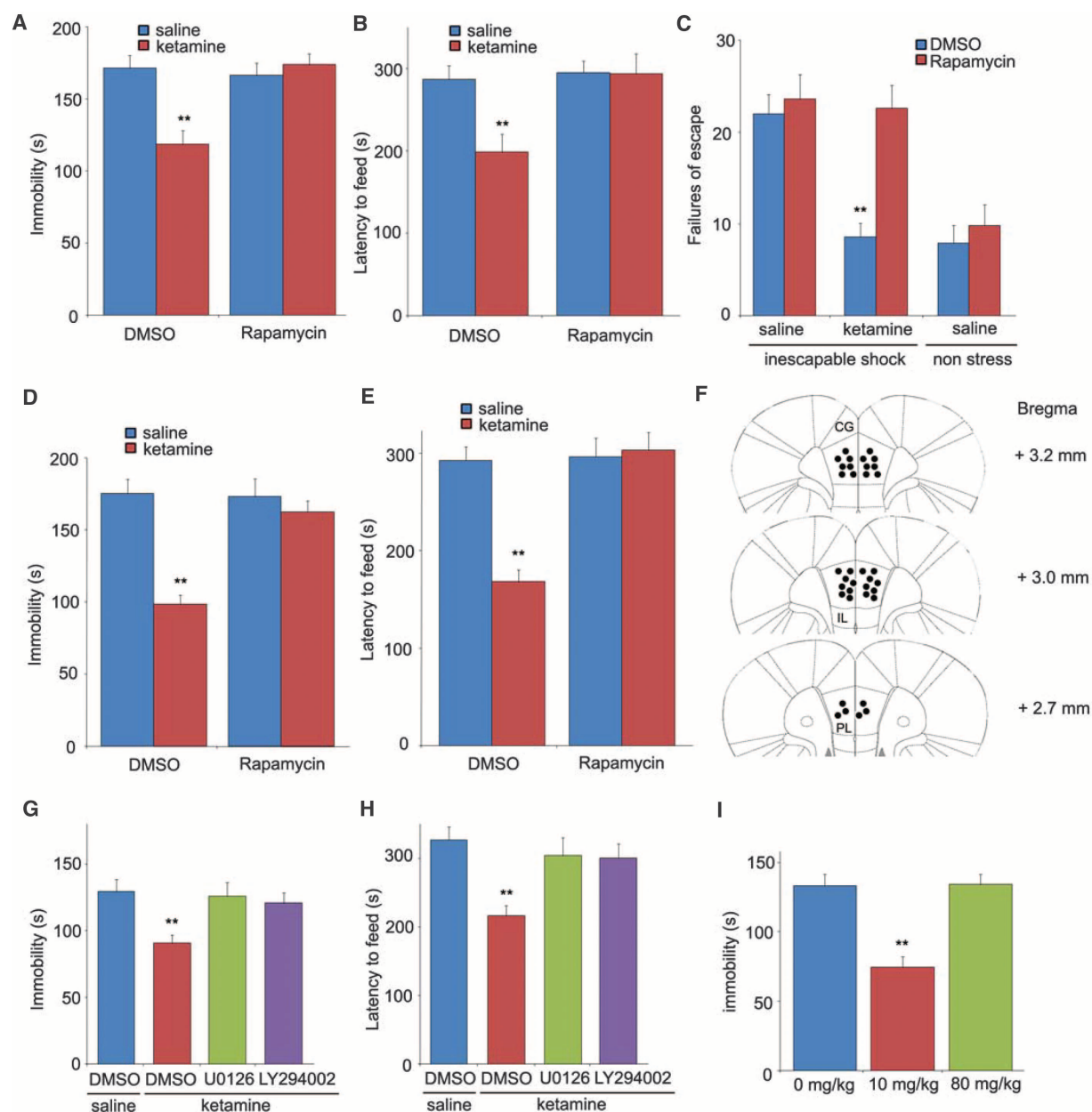
Results are the mean ± SEM (eight cells from four rats in each group; *$P < 0.05$; **$P < 0.01$, t test). (**E**) Ketamine enhanced mPFC layer V pyramidal cell EPSC responses. Sample whole-cell voltage-clamp recordings of 5-HT and hypocretin-induced EPSCs in slices (24 hours after Ketamine treatment). (**F**) Cumulative probability distributions showing significant increases in amplitude ($P < 0.0001$, Kolmogorov-Smirnov test-z value = 6.5 for 5-HT and 6.7 for Hcrt) and (**G**) frequency of 5-HT– and hypocretin-induced EPSCs (n = 12 neurons per group; *$P < 0.05$, t test). Ketamine induction of spine density and function were blocked by rapamycin infusions [(C) to (G)].

completely blocked the induction of phospho-rylated 4E-PB1, p70S6K, and mTOR, as well as ERK and Akt in the PFC (Fig. 1C and fig. S4). We assessed the possible involvement of ERK and Akt pathways in the activation of mTOR by intra-cerebroventricular (ICV) infusion of specific phar-macological antagonists. Inhibition of either ERK (U0126) or Akt [via inhibition of the upstream Akt activator phosphatidylinositol (PI3)-kinase by LY294002] blocked ketamine induction of phos-

phorylated 4E-BP1, p70567, and mTOR (Fig. 1D and fig. S5).

Activation of mTOR has been functionally linked with local protein synthesis in synapses, resulting in the production of proteins required for the formation, maturation, and function of new spine synapses (8). To determine whether ketamine induction of mTOR produces similar effects, we analyzed levels of several synaptic pro-teins in synaptoneurosomes from PFC. Ketamine

administration increased levels of the postsyn-aptic proteins PSD95 and GluR1, as well as the presynaptic protein synapsin I (Fig. 2, A and B). Ketamine-induced increases in these synaptic pro-teins was delayed relative to ERK, Akt, and mTOR, peaking at 2 to 6 hours, but remained elevated up to 72 hours. Ketamine also induced expres-sion of activity-regulated cytoskeletal-associated protein (Arc), with an intermediate (peak at 1 to 2 hours) but transient time course. The func-

Fig. 3. Rapid behavioral actions of ketamine require mTOR signaling. Rapamycin was infused (0.2 nmol, ICV) 30 min before ketamine (10 mg/kg, ip), and responses in the FST (**A**), NSFT (**B**), or LH (**C**) paradigms were determined. Values represent mean ± SEM (n = 6 to 8 animals; *P < 0.05; **P < 0.01; ANOVA). Infusion of rapamycin (0.01 nmol) into the mPFC blocked the anti-depressant actions of ketamine (10 mg/kg, ip) in the FST (**D**) and NSFT (**E**). (**F**) Location of rapamycin infusions in the PFC (infusion sites are the same on the right and left sides because of the use of bilateral cannulae). Pretreatment with inhibitors of ERK (U0126, 20 nmol, ICV) or PI3 kinase/Akt (LY294002, 20 nmol, ICV) blocked the behavioral effects of ketamine in FST (**G**) and NSFT (**H**). (**I**) Low (10 mg/kg) but not a high (80 mg/kg) anesthetic dose of ketamine produced an antidepressant action in the FST.

tional connection between mTOR activation and synaptic protein synthesis was examined by ICV infusion of selective mTOR inhibitor rapamycin, which completely blocked the induction of PSD95, GluR1, and synapsin I (Fig. 2B and fig. S6).

An increase in synapse-associated proteins indicates that ketamine administration rapidly increases synapse and spine formation. We therefore examined the influence of ketamine on spine number and morphology by two-photon imaging of the apical tuft of prelabeled layer V medial PFC (mPFC) pyramidal neurons. Analysis of the images shows that ketamine administration increased spine density in both distal and proximal segments of the apical tuft 24 hours after ketamine injection (Fig. 2, C and D). Ketamine also increased the population of mushroom (large-diameter) spines (fig. S7), an indication of increased spine maturation and synaptic strengthening (9). Synaptic strengthening is supported by analysis
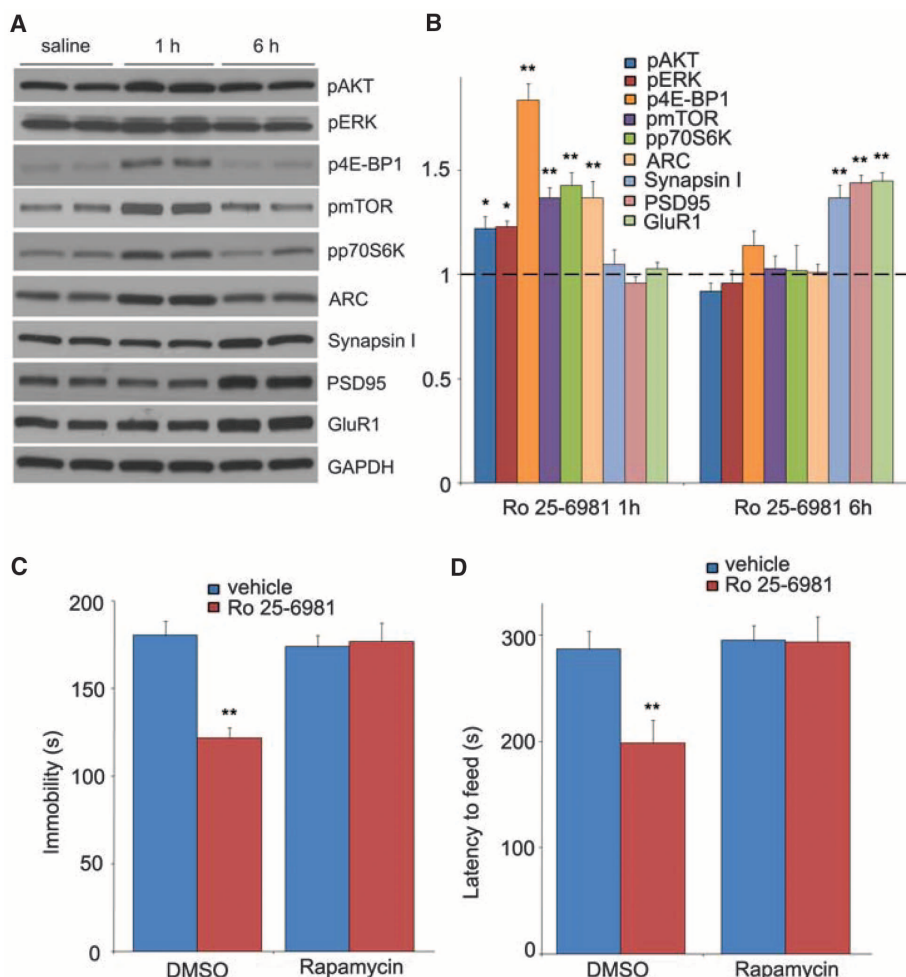
of the electrophysiological properties of the same cells, demonstrating that excitatory postsynaptic current (EPSC) frequency responses to serotonin [5-hydroxytryptamine (5-HT)], which are mediated predominantly by cortical-cortical synapses in the apical tuft (10), are significantly increased by ketamine administration (Fig. 2, E to G). Responses to hypocretin and orexin, which occur selectively at apical thalamocortical synapses (11), are also increased (Fig. 2, E to G). In both cases, there is a significant increase in EPSC amplitude (Fig. 2F), consistent with the elevation in mushroom spines (fig. S7) and GluR1. Ketamine induction of spines and 5-HT and hypocretin-stimulated excitatory postsynaptic potentials (EPSPs) are blocked by infusion of rapamycin (Fig. 2, C to G, and fig. S7).

We next determined whether activation of mTOR signaling is required for the antidepressant behavioral actions of ketamine. As previously reported, a low dose of ketamine produced a

rapid antidepressant effect in two well-established behavioral models of despair, the forced swim test (FST) and learned helplessness (LH) in response to inescapable stress (IES), as well as a model of anxiety, the novelty suppressed feeding test (NSFT) (Fig. 3, A to C). Traditional antidepressants are effective in these tests after acute (1 day, FST), subchronic (6 days, LH), and chronic (21 days, NSFT) treatment, whereas a single dose of ketamine was effective in all three tests. Moreover, infusion (ICV) of rapamycin completely abolished the antidepressant actions of ketamine in all three tests (Fig. 3, A to C). The role of mTOR signaling in the actions of ketamine was further examined by local infusion of rapamycin into the mPFC, which resulted in a complete blockade of the behavioral effects of ketamine in FST and NSFT tests (Fig. 3, D and E) (location of rapamycin infusions into the mPFC is shown in Fig. 3F). The effects of inhibitors of ERK and PI3k/Akt, which mediate ketamine induction of mTOR, were also examined. Infusion (ICV) of selective ERK (U0126) or PI3k/Akt (LY294002) inhibitors blocked the antidepressant actions of ketamine in the FST and NSFT (Fig. 3, G and H). Lastly, the behavioral actions of ketamine in the FST occurred with a dose-response profile similar to that for induction of ERK, Akt, and mTOR (Fig. 3I). This addresses a major point of discussion in the field as to whether an anesthetic dose of ketamine could produce an antidepressant effect.

Basic research and clinical studies demonstrate that stress and depression can cause atrophy of PFC pyramidal neurons in rodent models and in postmortem tissue of depressed subjects (10, 12), and brain-imaging studies report a decrease in PFC volume in depressed patients (13). Exposure to stress in the LH paradigm decreased levels of synaptic proteins GluR1, PSD95, and synapsin I, and a single dose of ketamine reversed this deficit in a rapamycin-sensitive manner (fig. S8). These results indicate that ketamine induction of synapse-associated protein synthesis provides a mechanism for rapid reversal of stress- and/or depression-mediated deficits and could enhance PFC-mediated connectivity and function.

Ketamine is a psychotomimetic drug with abuse potential, and a more selective agent would be desirable for clinical antidepressant use. There have been reports that selective NMDA receptor subunit 2B (NR2B) antagonists produce antidepressant actions similar to ketamine in both preclinical models and clinical trials (7, 14). Therefore, we examined the influence of Ro 25-6981, a NR2B-selective compound, on mTOR signaling and rapamycin-sensitive behaviors. Ro25-6981, at a dose (10 mg/kg) identified in the FST to be optimal (fig. S9), produced a transient activation of mTOR signaling (increased phosphorylation of 4E-BP1, p70S6K, and mTOR), as well as ERK and Akt signaling in synaptoneurosomes from PFC (Fig. 4, A and B). Ro 25-6981 administration also increased levels of the synaptic proteins Arc, PSD95, GluR1, and synapsin I in synaptoneurosomes (Fig. 4, A and

Fig. 4. Selective NR2B antagonist Ro 25-6981 activates mTOR signaling and produces rapamycin-sensitive behavioral effects. (**A** and **B**) Effects of Ro 25-6981 (10 mg/kg, ip) on pmTOR, p4E-BP1, pp70S6K, pERK, pAkt, Arc, synapsin I, PSD95, and GluR1 in PFC. (**C** and **D**) Pretreatment with rapamycin (0.2 nmol, ICV) abolished the actions of Ro 25-6981 in FST (C) and NSFT (D). Values represent mean ± SEM (n = 6 to 8 animals; *P < 0.05; **P < 0.01; ANOVA).

B). Induction of Arc was more rapid and transient, whereas PSD95, GluR1, and synapsin I were delayed, similar to the delay observed after ketamine administration. Lastly, Ro 25-6981 administration produced rapid antidepressant effects (24 hours) in the FST and NSFT, which were blocked by preinfusion (ICV) of rapamycin (Fig. 4, C and D).

Fast activation of mTOR signaling resulting in rapid and sustained elevation of synapse-associated proteins and spine number in the PFC represents a mechanism for the rapid antidepressant actions of ketamine. These effects result in elevated 5-HT neurotransmission, a primary target of traditional antidepressants, although the latter can take weeks or months to induce a therapeutic response (2). The mechanisms underlying the induction of mTOR signaling are unclear, but the requirement for glutamate-AMPA receptor activation is consistent with the hypothesis that there is a subset of NMDA receptors, possibly on γ-aminobutyric acid (GABA)–releasing interneu-

rons, that when antagonized, block GABA release lead to disinhibition of glutamate signaling (15). Further characterization of these actions of NMDA receptor blockade and the signaling pathways that stimulate mTOR signaling and mediate the rapid induction of synapses in the PFC will provide novel therapeutic targets for antidepressant drug development.

References and Notes

1. R. C. Kessler et al., JAMA **289**, 3095 (2003).
2. M. H. Trivedi et al., Am. J. Psychiatry **163**, 28 (2006).
3. R. M. Berman et al., Biol. Psychiatry **47**, 351 (2000).
4. C. A. Zarate Jr. et al., Arch. Gen. Psychiatry **63**, 856 (2006).
5. J. H. Krystal, Swiss Med. Wkly. **137**, 215 (2007).
6. Materials and methods are available as supporting material on Science Online.
7. S. Maeng et al., Biol. Psychiatry **63**, 349 (2008).
8. C. A. Hoeffer, E. Klann, Trends Neurosci. **33**, 67 (2010).
9. Y. Yoshihara, M. De Roo, D. Muller, Curr. Opin. Neurobiol. **19**, 146 (2009).
10. R. J. Liu, G. K. Aghajanian, Proc. Natl. Acad. Sci. U.S.A. **105**, 359 (2008).
11. E. K. Lambe, G. K. Aghajanian, Neuroscience **145**, 900 (2007).
12. G. Rajkowska et al., Biol. Psychiatry **45**, 1085 (1999).
13. W. C. Drevets, Annu. Rev. Med. **49**, 341 (1998).
14. S. H. Preskorn et al., J. Clin. Psychopharmacol. **28**, 631 (2008).
15. N. B. Farber, J. W. Newcomer, J. W. Olney, Prog. Brain Res. **116**, 421 (1998).
16. This work is supported by U.S. Public Health Service grants MH45481 and 2P01 MH25642 and by the Connecticut Mental Health Center.

Females Use Multiple Mating and Genetically Loaded Sperm Competition to Target Compatible Genes

Sarah R. Pryke, Lee A. Rollins, Simon C. Griffith*

Individuals in socially monogamous species may participate in copulations outside of the pair bond, resulting in extra-pair offspring. Although males benefit from such extra-pair behavior if they produce more offspring, the adaptive function of infidelity to females remains elusive. Here we show that female participation in extra-pair copulations, combined with a genetically loaded process of sperm competition, enables female finches to target genes that are optimally compatible with their own to ensure fertility and optimize offspring viability. Such female behavior, along with the postcopulatory processes demonstrated here, may provide an adaptive function of female infidelity in socially monogamous animals.

In socially monogamous species, optimal female mate choice is constrained by the number of high-quality or compatible social partners available. Extra-pair sexual relationships provide an opportunity for females to ensure against the fitness costs of genetically incompatible social partnerships and to improve the genetic quality of at least some of their offspring by mating with extra-pair males that are either genetically more compatible or of higher genetic quality than their social partner (1–3). To date, studies investigating the potential additive genetic benefits provided by extra-pair males have generally either failed to

detect effects or have reported only weak or inconsistent results (4–6). However, most studies have inferred female infidelity through the forensic molecular analysis of the outcome of fertilization (i.e., paternity), and with few exceptions (7), have not considered female copulatory behavior, including the number of partners and the distribution of copulations among them. Therefore, it has been difficult to gain insight into the underlying postcopulatory processes, and ultimately, to determine the adaptive function of female polyandry in socially monogamous animals.

In the socially monogamous Gouldian finch (Erythrura gouldiae), genetic incompatibility between interbreeding red and black head-color morphs (that is, different genotypes) results in high offspring mortality rates (more than 60% greater mortality from egg to sexual maturity than compatible pairs of the same head color) (8).

Mate compatibility is signaled by head color, which is determined by a Z-linked gene: Females are hemizygous for this gene (Z^r black, Z^R red), whereas male genotypes can be homozygous $Z^r Z^r$ (black), $Z^R Z^R$ (red), or heterozygous $Z^R Z^r$ (red). Individuals demonstrate precopulatory mate preferences for their own morph type; however, perhaps because of constraints on preferred-mate availability, up to 30% of breeding pairs in wild populations are mixed morph (9).

We tested for adaptive female participation in extra-pair copulations by presenting captive female Gouldian finches breeding in genetically compatible (social partner of the same genotype) and incompatible social pairs (social partner of different morph), with an opportunity to seek an extra-pair copulation with either a compatible or incompatible male (10). On the day after the female-initiated egg laying (day 1; day 0 = day the first egg is laid), the birds in the social pair were physically and visually separated by an opaque divider, which split the cage in half, and a virgin male in breeding condition was placed with the female for 60 min. In the context of selection for compatible genes (1), this experimental design provided a predicted adaptive context (incompatible social partner and compatible extra-pair partner), a maladaptive context (compatible social partner and incompatible extra-pair partner), and two selectively neutral situations (both social and extra-pair partners either incompatible or compatible) (Fig. 1).

Despite morph-assortative mate preferences (9) and selection against mixed morph mating (11), surprisingly, females across all experimental contexts were equally likely to engage in extra-pair behavior [$\chi^2 = 0.87$, degrees of freedom (df) = 3, $P = 0.83$]. Overall, 77.5% (31 of 40) of females copulated with the extra-pair male (Fig. 1). All

Department of Biological Sciences, Macquarie University, Sydney, NSW 2109, Australia.

*To whom correspondence should be addressed. E-mail: simon.griffith@mq.edu.au